

# Laser Refrigeration by an Ytterbium-Doped NaYF<sub>4</sub> Microspinner

Elisa Ortiz-Rivero, Katarzyna Prorok, Inocencio Rafael Martín, Radostaw Lisiecki, Patricia Haro-González,\* Artur Bednarkiewicz, and Daniel Jaque\*

Thermal control of liquids with high (micrometric) spatial resolution is required for advanced research such as single molecule/cell studies (where temperature is a key factor) or for the development of advanced microfluidic devices (based on the creation of thermal gradients at the microscale). Local and remote heating of liquids is easily achieved by focusing a laser beam with wavelength adjusted to absorption bands of the liquid medium or of the embedded colloidal absorbers. The opposite effect, that is highly localized cooling, is much more difficult to achieve. It requires the use of a refrigerating micro-/nanoparticle which should overcome the intrinsic liquid heating. Remote monitoring of such localized cooling, typically of a few degrees, is even more challenging. In this work, a solution to both problems is provided. Remote cooling in D<sub>2</sub>O is achieved via anti-Stokes emission by using an optically driven ytterbium-doped NaYF<sub>4</sub> microparticle. Simultaneously, the magnitude of cooling is determined by mechanical thermometry based on the analysis of the spinning dynamics of the same NaYF<sub>4</sub> microparticle. The angular deceleration of the NaYF<sub>4</sub> particle, caused by the cooling-induced increase of medium viscosity, reveals liquid refrigeration by over −6 K below ambient conditions.

the design and development of remotely activated heating and cooling units of micrometric dimensions. Not only that – temperature needs also to be monitored in real time so that this heating/cooling should provide real time temperature feedback to, for instance, prevent unintentional damage in biological systems. Materials science and sensing technologies are being joined together to develop contactless thermal microsenors capable of remote heating and cooling.

Lanthanide-doped sodium yttrium fluoride (NaYF<sub>4</sub>: Ln) micro/nanocrystals have been considered as one of the most important and promising building blocks of modern photonics.<sup>[5,6]</sup> Their physical properties, including their nonstoichiometric composition,<sup>[7,8]</sup> are well-studied and they are being used in a wide range of applications including bioimaging,<sup>[9,10]</sup> remote sensing,<sup>[11–14]</sup> imaging displays, solar cells<sup>[15–17]</sup> and photocatalysis.<sup>[18,19]</sup> Most of these appli-

cations are based on the good fluorescent properties (i.e., high (photo)stability, high brightness, spectral purity and long fluorescence lifetimes) of lanthanide ions in the NaYF<sub>4</sub> lattice.<sup>[20]</sup> After optical excitation, lanthanide ions in NaYF<sub>4</sub> undergo relaxation to their ground state by involving both radiative and non-radiative de-excitations. In most of the cases, the presence of non-radiative transitions, by multi-phonon relaxation (MPR), results in relevant heating of the NaYF<sub>4</sub>: Ln system through vibrations of ligands and solvent molecules.<sup>[21,22]</sup> The situation may occur differently when doping such crystals with ytterbium ions.

## 1. Introduction

Despite technological advances, accurate control of the temperature remains a challenge to these days. While it is less arduous at large scale, this control is especially complicated when it has to be achieved remotely (in a contactless manner) and confined on the micro- and nanoscales. However, such an advanced spatial control over temperature is necessary in numerous fields ranging from the study of cell dynamics<sup>[1,2]</sup> to the development of new microfluidic devices.<sup>[3,4]</sup> These applications require

E. Ortiz-Rivero, P. Haro-González, D. Jaque  
Nanomaterials for Bioimaging Group  
Departamento de Física de Materiales  
Facultad de Ciencias  
Universidad Autónoma de Madrid  
Madrid 28049, Spain  
E-mail: patricia.haro@uam.es; daniel.jaque@uam.es

 The ORCID identification number(s) for the author(s) of this article can be found under <https://doi.org/10.1002/smll.202103122>.

© 2021 The Authors. Small published by Wiley-VCH GmbH. This is an open access article under the terms of the Creative Commons Attribution License, which permits use, distribution and reproduction in any medium, provided the original work is properly cited.

DOI: 10.1002/smll.202103122

E. Ortiz-Rivero, P. Haro-González, D. Jaque  
Instituto de materiales Nicolás Cabrera  
Universidad Autónoma de Madrid  
Madrid 28049, Spain  
K. Prorok, R. Lisiecki, A. Bednarkiewicz  
Institute of Low Temperature and Structure Research  
Polish Academy of Sciences  
Okólna 2, Wrocław 50-422, Poland

I. R. Martín  
Departamento de Física  
Universidad de La Laguna  
Apdo. 456, San Cristóbal de La Laguna E-38200, Spain

I. R. Martín  
Instituto Universitario de Materiales y Nanotecnología (IMN)  
Universidad de La Laguna  
Apdo. 456, San Cristóbal de La Laguna E-38200, Spain

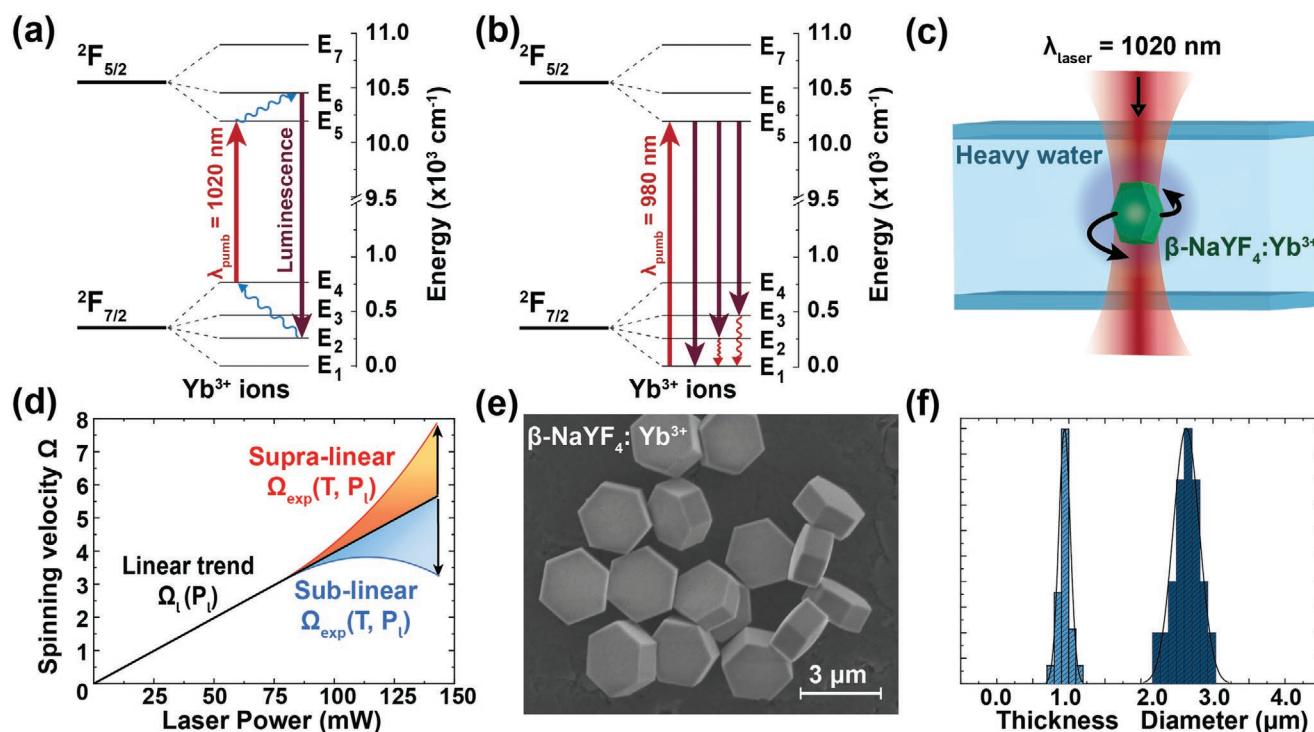


**Figure 1.** Energy levels diagram of Yb<sup>3+</sup> ions in NaYF<sub>4</sub> indicating a) the cooling mechanism (phonon absorption) when optically excited at 1020 nm and b) the heating mechanism (phonon emission) when excited at 980 nm. c) Schematic representation of the experimental set-up, where an hexagonal disk-shaped particle in heavy water is optically trapped and rotated with a 1020 nm laser beam. d) Graphic representation of the spinning velocity as a function of laser power for a constant temperature (linear trend represented by black line), in presence of laser-induced heating (red line) and in presence of laser-induced cooling (blue line). e) SEM image of the hexagonal disk-shaped particles used all along this work. Scale bar is 3  $\mu\text{m}$ . f) Size distribution of the 5 at% ytterbium-doped NaYF<sub>4</sub> microparticles.

They are exceptional, not only because their simple energy level scheme reduces the possibility of cross relaxation events (Figure 1a), but also because their high absorption cross sections at  $\approx 980 \text{ nm}$  has been successfully used to sensitize and improve the efficiency of upconversion emission from co-doped activator ions such as Er<sup>3+</sup>, Tm<sup>3+</sup>, Ho<sup>3+</sup>, etc.<sup>[23]</sup> Interestingly, in singly Yb<sup>3+</sup> doped materials, the combination of the energy scheme of ytterbium ions with appropriate photoexcitation wavelengths facilitates the process known as optical cooling. Optical cooling is based on low energy pumping photons (corresponding to long wavelength photoexcitation) matching the closest Stark components of the ground and excited multiplets ( $E_4 \rightarrow E_5$  transition, corresponding to an excitation wavelength of 1020 nm, as represented in Figure 1a) that, on average, may result in the emission of photons with larger energies (i.e., shorter wavelengths) than that of the excitation beam.<sup>[24,25]</sup> In such case, when the energy of the emitted photon exceeds the energy of the absorbed photon and the energy difference is balanced by the absorption of host matrix phonons, net cooling has been observed (Figure 1a). Laser cooling of ytterbium-doped bulk materials (i.e., crystals and glasses) has been predicted and demonstrated,<sup>[26–30]</sup> first by R. I. Epstein et al. in bulk ZBLANP:Yb<sup>3+</sup>.<sup>[31]</sup> Ytterbium-doped nano- and microparticles have been also trapped and cooled in low pressure chambers,<sup>[32]</sup> but achieving similar effects on micro/nanoparticles suspended in liquids without sophisticated chambers and high quality vacuum is much more challenging. This is due to the presence of medium-related partial absorption of laser radiation

together with the presence of large volume heat sinks and the reduced cooling power that is consequence of the small amount of laser power absorbed. Indeed, the demonstrations of liquid laser refrigeration, especially important for further studying physiological processes in vitro, by ytterbium-doped particles are scarce (see Table S1, Supporting Information). In these rare cases, liquid cooling was monitored indirectly by analyzing either the luminescence or the Brownian dynamics of the trapped particles.<sup>[6,33]</sup> or by using optomechanical cantilevers.<sup>[34]</sup> Thermal reading by luminescence requires the inclusion of an additional lanthanide ion (e.g., erbium) that besides reporting the temperature, can unfortunately induce additional nonradiative pathways and, hence, may become a undesired heating source. On the other hand, monitoring temperature by Brownian motion analysis requires sophisticated optical setups (quadrant photodiodes and fast data acquisition and analysis) and typically leads to unacceptable temperature uncertainties of a few degrees. Finally, bare Yb<sup>3+</sup> luminescence ratiometric temperature readout<sup>[32]</sup> requires relatively high resolution spectra recording, which is hindered both by costly and complicated optical setups as well as by the sensitivity drop of charge-coupled device (CCD), complementary metal oxide semiconductor (CMOS), or most photomultiplier (PMT) detectors in the NIR region, where Yb<sup>3+</sup> emits. Therefore, new, straightforward, direct and simple approaches for reliable thermal monitoring during laser refrigeration in liquids are desirable.

The NaYF<sub>4</sub> host matrix is not only a material of choice for Ln<sup>3+</sup> ions doping because of the reliable and reproducible

methods to synthesize nano- and microcrystals of well-controlled morphology and narrow size distribution.<sup>[35,36]</sup> It also presents interesting optical properties. NaYF<sub>4</sub> refractive index is 1.46,<sup>[37,38]</sup> which leads to a relevant index contrast ( $\Delta n$ ) when suspended, for instance, in water. This makes optical manipulation of NaYF<sub>4</sub>: Ln micro/nanoparticles feasible. Simultaneous optical manipulation and luminescence analysis of a single NaYF<sub>4</sub>: Er<sup>3+</sup>, Yb<sup>3+</sup> particle has already been used for thermal scanning in the surroundings of a living cell<sup>[39]</sup> or the successful demonstration of the possibility to trap single colloidal nanoparticles.<sup>[40]</sup> Furthermore, NaYF<sub>4</sub> is a birefringent material so laser-to-particle transfer of angular momentum could occur. Indeed, when a NaYF<sub>4</sub> microparticle is optically trapped with circularly polarized radiation, it behaves as a spinner (Figure 1c), whose spinning velocity has been demonstrated to be susceptible to environmental conditions or biospecific detection reactions.<sup>[41,42]</sup>

In addition to their practical applications, such as micro-mixing in integrated reactors,<sup>[43]</sup> optically driven spinners have also emerged as a new class of contactless microthermometers.<sup>[41]</sup> The steady spinning velocity of a single NaYF<sub>4</sub> crystal,  $\Omega(T, P_l)$ , is defined as

$$\Omega(T, P_l) = \beta \cdot \frac{P_l}{\eta(T)} \quad (1)$$

where  $\beta$  is a constant that depends on the geometry of the particle and its birefringence,  $P_l$  is the applied laser power, and  $\eta(T)$  is the medium viscosity at temperature  $T$ . When the NaYF<sub>4</sub> microspinner is operating in a medium exhibiting strongly temperature-dependent viscosity (such as heavy water, see Supporting Information), its spinning dynamics are strongly determined by the local temperature. In the ideal case, where the liquid temperature remains constant and independent of the laser power, the liquid viscosity is constant and  $\Omega$  increases linearly with  $P_l$  (Figure 1d). If laser radiation locally heats the liquid, its viscosity decreases, enabling the spinning velocity to increase. Thus, in presence of laser-induced heating, the  $\Omega(T, P_l)$  velocity displays a supralinear relation with  $P_l$  (Figure 1d). The analysis of this supralinear relation has already been used to monitor the remote laser heating of liquids.<sup>[44]</sup> Similar arguments can be, in principle, used to detect laser-induced refrigeration. In this case, cooling would be evidenced by a sublinear  $\Omega(T, P_l)$  versus  $P_l$  relation because the liquid viscosity increases when cooling (Figure 1d). Nevertheless, the use of an optically driven spinner to induce and monitor laser refrigeration in liquids still remains as an unexplored possibility.

In this work, a single ytterbium-doped NaYF<sub>4</sub> micron size particle with various concentration of Yb<sup>3+</sup> ions has been trapped and rotated by a circularly polarized laser beam. Their spinning velocities have been measured as a function of the laser power so that the liquid's local temperature was elucidated based on their deviation from linearity. Relevant laser refrigeration of liquid in close proximity to the NaYF<sub>4</sub>: 5% Yb<sup>3+</sup> microparticle was found when pumping with wavelength (1020 nm) longer than the average fluorescence wavelength (980 nm). The magnitude of laser refrigeration has been studied as a function of both ytterbium content and laser power. The results have been compared with previous works and discussed in terms of the spectroscopic properties of ytterbium ions in NaYF<sub>4</sub>.

## 2. Results and Discussion

Figure 1e shows a representative scanning electron microscope (SEM) image of the NaYF<sub>4</sub>: Yb<sup>3+</sup> microcrystals used all along this work. Details about the synthesis procedure can be found in the Experimental Section. The size histogram obtained from the analysis of SEM images corresponding to the 5% doping level of Yb<sup>3+</sup> is shown in Figure 1f revealing an average thickness and diameter of  $0.9 \pm 0.1$  and  $2.6 \pm 0.2$   $\mu\text{m}$ , respectively. The experimental set-up used for laser-induced spinning is schematically represented in Figure 1c and is fully described in the Experimental Section. Briefly, the NaYF<sub>4</sub>: Yb<sup>3+</sup> microcrystals were dispersed in D<sub>2</sub>O at a very low concentration to avoid multiple particle trapping. The solution was introduced into a 120  $\mu\text{m}$  tall microchannel. Optical trapping and spinning were induced by a single-mode fiber coupled laser diodes operating at either 980 or 1020 nm. Both lasers were circularly polarized by a quarter waveplate. In order to determine the spinning velocity  $\Omega(T, P_l)$ , a quadrant photodiode was used to detect transmitted/scattered light periodicity, which is much simpler and more accurate than using Brownian motion movements. The critical difference between the two lasers used in this work is their operating wavelength that is correspondingly shorter or longer than the averaged emission wavelength of ytterbium ions in NaYF<sub>4</sub> ( $\lambda_{\text{av}} \approx 990$  nm, see Section 3 in the Supporting Information for details on how it is calculated).

Figure 2a shows the absorption spectra of pure D<sub>2</sub>O and of the undoped NaYF<sub>4</sub> microcrystals, which obviously does not contain the ytterbium absorption band at 980 nm. Because 980 nm radiation is neither absorbed by the NaYF<sub>4</sub> microcrystal nor by the medium, no laser-induced heating is expected during optical spinning. In these conditions, a linear  $\Omega$  versus  $P_l$  relationship is expected, a fact that has been experimentally corroborated (Figure 2b). When the laser wavelength is switched to 1020 nm, a slight absorption of D<sub>2</sub>O medium does exist, although, according to previous works, it is expected to cause a negligible local heating ( $< 0.1$  K for a laser power of 200 mW).<sup>[45]</sup> In this case, we again expect a linear trend of  $\Omega$  versus  $P_l$  for an undoped NaYF<sub>4</sub> microcrystal in D<sub>2</sub>O as, indeed, has been experimentally observed (Figure 2c). The situation becomes completely different when dealing with ytterbium-doped NaYF<sub>4</sub> particles. Figure 2d shows the absorption spectrum of a 5% ytterbium-doped NaYF<sub>4</sub> microcrystal that is characterized by the relatively broad absorption band corresponding to the  $^2F_{7/2} \rightarrow ^2F_{5/2}$  transition. Ytterbium ions absorb most efficiently at 980 nm as this matches the zero-phonon line ( $E_1 \rightarrow E_5$  transition, Figure 1b). The subsequent nonradiative transitions induce relevant heating of the NaYF<sub>4</sub> microcrystal. Laser-induced heating decreases the medium viscosity and induces a supralinear  $\Omega$  versus  $P_l$  trend, as experimentally observed (Figure 2e). However, when using 1020 nm excitation, the activation of phonon absorption to reach an energy balance between pump and fluorescence photons induces local refrigeration, as previously discussed (Figure 1a). Local refrigeration increases the medium viscosity that, accordingly to expression (1), activates particle deceleration and reduces the spinning velocity. The sublinear  $\Omega$  versus  $P_l$  relation expected in the presence of laser-induced

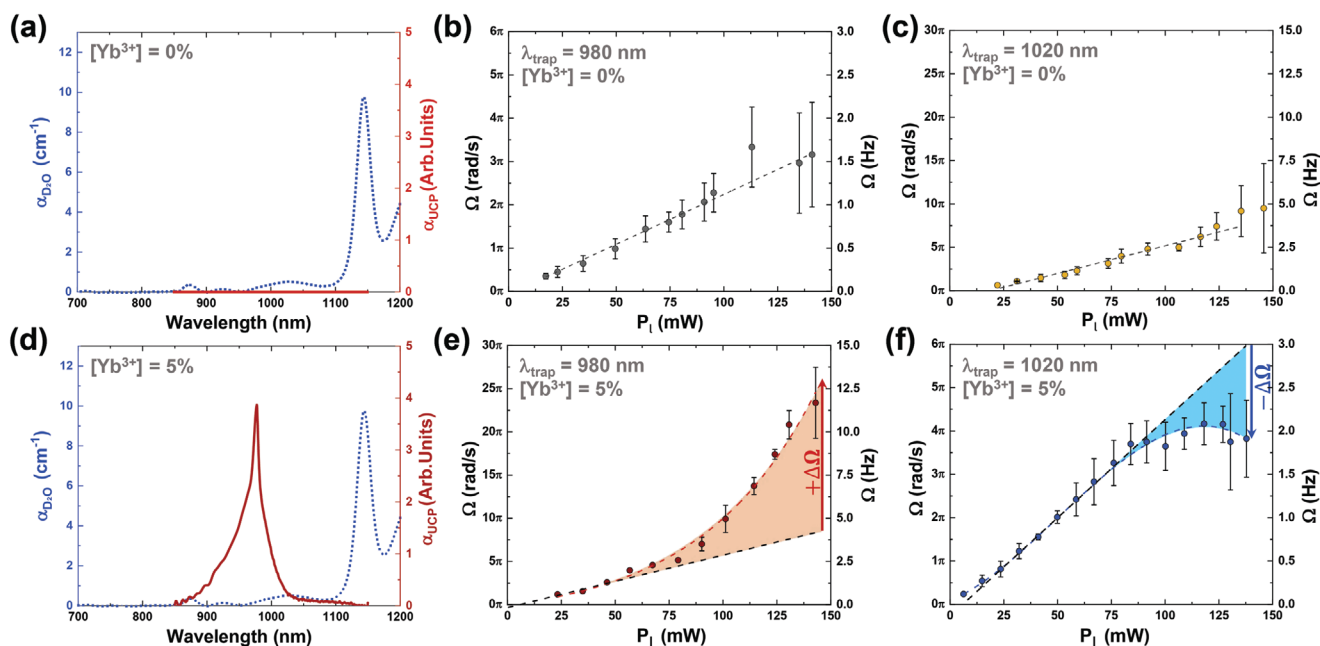


**Figure 2.** Absorption spectrum of both, pure medium (heavy water, blue dots) overlapping the absorption spectra of undoped and 5%Yb<sup>3+</sup>-doped NaYF<sub>4</sub> microparticles in the medium (red lines) ((a) and (d), respectively). (b) and (c) include the power dependence of the spinning velocity ( $\Omega$ ) of an undoped NaYF<sub>4</sub> microparticle as obtained under 980 and 1020 nm laser photoexcitation, respectively. The spinning velocity increases linearly with the laser power, indicating the absence of relevant temperature change. (e) and (f) show the power dependence of the spinning velocity ( $\Omega_{\text{exp}}(P_i)$ ) of the 5 at% Yb<sup>3+</sup>-doped NaYF<sub>4</sub> microparticle as obtained under 980 and 1020 nm laser photoexcitation, respectively. The spinning velocities versus laser power deviate from the low-power linear dependence (dashed lines), being supralinear for 980 nm, whereas it shows a clear sublinear trend for 1020 nm photoexcitation.

refrigeration has been, indeed, corroborated experimentally as it can be observed in Figure 2f.

Experimental data included in Figure 2e,f reveals laser heating/refrigeration in the surroundings of a NaYF<sub>4</sub>: Yb<sup>3+</sup> microspinning optically driven by 980/1020 nm radiation, respectively. Experimental data also allow to quantify the magnitude of such heating and cooling. For a quantitative analysis of the  $\Omega$  versus  $P_i$  curves we denote  $\Omega_{\text{exp}}(P_i)$  as the experimentally determined spinning velocity for a laser power  $P_i$  and  $\Omega_i(P_i)$  as the expected spinning velocity in the linear regime (i.e., assuming a constant liquid temperature and equal to  $RT = 293.15$  K). For the low range of laser power (where laser heating/cooling of the medium is negligible), the experimentally obtained spinning velocities can be linearly extrapolated and serve as the room temperature reference for all other higher laser intensities. Once the  $\Omega_i(P_i)$  and  $\Omega_{\text{exp}}(P_i)$  are known, we define the relative change of spinning velocity for a given laser power,  $P_i$ ,  $\Delta\Omega_r(P_i)$ , as:

$$\Delta\Omega_r(P_i) = \frac{\Omega_{\text{exp}}(P_i) - \Omega_i(P_i)}{\Omega_i(P_i)} \quad (2)$$

A graphical representation of how  $\Omega_i(P_i)$  and  $\Omega_{\text{exp}}(P_i)$  are defined is included in Figure 1d. According to expression (1), this can be correlated with the relative change between the medium viscosity at  $RT$  and the medium viscosity at the local medium temperature allowing to predict how the spinner is rotating at larger laser intensities and thus can exploit the deviation from this predicted behaviour as the signature of heating or cooling. In order to correlate the value  $\Delta\Omega_r(P_i)$  obtained from

experimental data with the actual temperature of the spinning particle we need to build up a calibration curve. Details on how this calibration curve is obtained can be found in the Supporting Information. Briefly, we measured, for a fixed low laser power, the spinning velocity of the ytterbium-doped microspinning at different temperatures ( $\Omega_i(T)$ ) and calculate the relative change of spinning velocity at each temperature ( $\Delta\Omega_r(T)$ ) in respect to room temperature ( $RT$ , 293.15 K). Since  $\Omega_i(P_i)$  is the spinning velocity in absence of laser induced heating/cooling, it corresponds to the spinning velocity at room temperature (i.e.,  $\Omega_i(P_i) = \Omega_i(RT)$ ). The relative change in the spinning velocity induced by laser radiation of power  $P_i$  due to the induced change in local temperature from  $RT$  up to  $T_i(P_i)$  is given by:

$$\Delta\Omega_r(T) = \frac{\Omega_i(T) - \Omega_i(RT)}{\Omega_i(RT)} \quad (3)$$

Figure 3a shows the calibration curve obtained according to equation (3). The procedure to determine the variation of the temperature of the spinning particle with the laser power is first to determine  $\Delta\Omega_r(P_i)$  from experimental data. Then, this relative change in the spinning velocity is translated into temperature by using the calibration curve of Figure 3a.

It should be noted at this point that the translation of the change in spinning velocity into temperature is done on the basis of a calibration curve built up by considering the change in the temperature-induced angular velocity of a spinning particle in a homogeneous medium with a constant temperature and a constant viscosity. But, when dealing with an optically



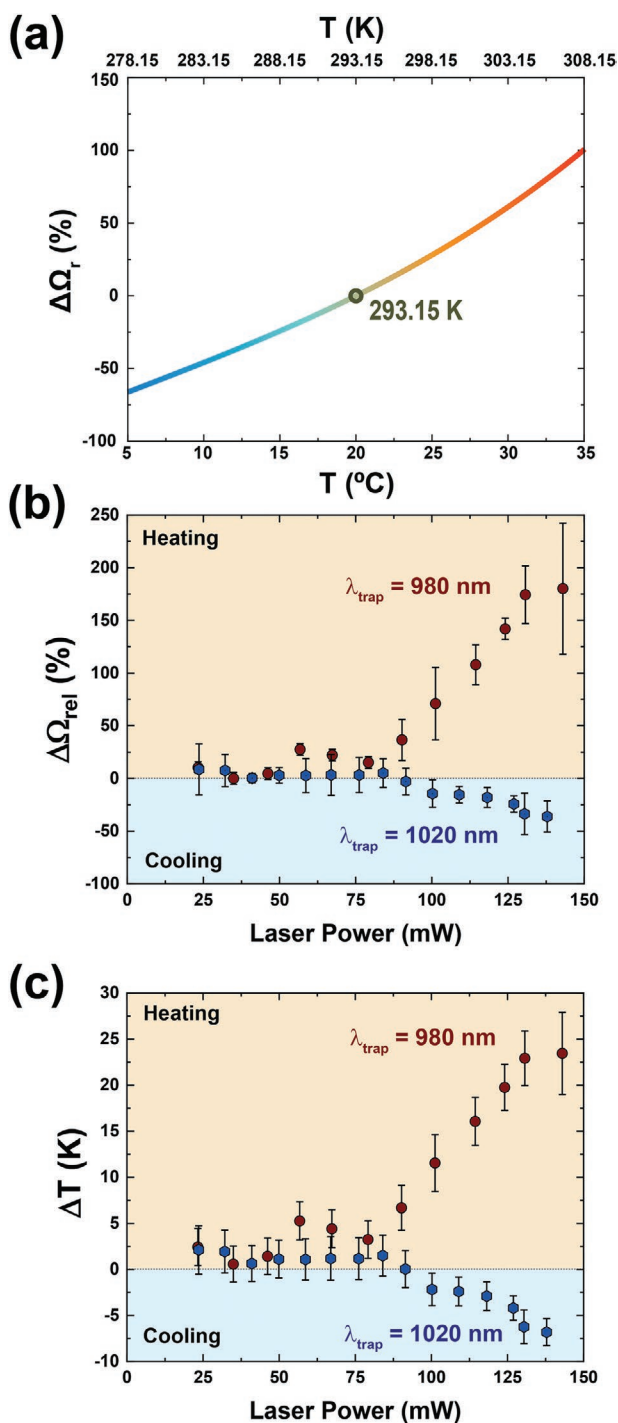


**Figure 3.** a) Relative change of the angular velocity of a NaYF<sub>4</sub>: 5% Yb<sup>3+</sup> microspinner in respect to that at 293.15 K in homogenous calibration. Note that heating leads to an increment in the angular velocity whereas cooling causes an angular deceleration. b) Deviation from linearity of the spinning velocity of a 5 at% ytterbium-doped NaYF<sub>4</sub> microparticle as obtained under 980 and 1020 nm laser manipulation. Under 980 nm pumping wavelength, the increment in the spinning velocity indicates heating, whereas the reduction in spinning velocity evidenced under 1020 nm reveals the presence of cooling. (c) shows the power-dependent temperature increment of the spinning particle under 980 nm and 1020 nm laser manipulation, respectively. Data were derived from (b) by using the calibration curve of (a).

driven spinner in presence of local heating or cooling, this is not the situation. Temperature and viscosity gradients are created around the rotating particle. The rotation of the particle would be affected by an “effective” viscosity and the temperatures estimated in this work would correspond to an “effective” temperature resulting from an average between the particle’s temperature and chamber temperature. Therefore, the here reported cooling magnitudes are, indeed, lower bounds of the cooling produced within the particle. Despite these differences in homo- and heterogeneity of the microenvironment at microscopic scale, our model seems to work sufficiently well and enabled to evaluate the cooling behavior.

For the quantification of the local temperature we first determine the value of  $\Delta\Omega_r$  (from data included in Figures 2e,f) for each laser power (Figure 3b). These can be translated into temperature by using the ‘calibration data’ included in Figure 3a, as it is described in SI. The resulting variation of local temperature versus laser power data, corresponding to the 5 at% doped NaYF<sub>4</sub>: Yb<sup>3+</sup> microparticle, are shown in Figure 3c. It is therefore obtained that, for the maximum pump power of 137 mW, the 980 nm excited NaYF<sub>4</sub>: Yb<sup>3+</sup> microparticle heats the surrounding medium by more than 20 K. On the other hand, anti-Stokes excitation at 1020 nm induces a laser refrigeration of the surrounding medium close to −6.8 K at the same pump power (137 mW).

In a first order approximation, the temperature increment of an individual microparticle surrounded by a medium with thermal conductivity  $\kappa$  is given by<sup>[46]</sup>

$$\Delta T = \frac{q}{4\pi\kappa R_e} \quad (4)$$

where  $q$  is the heating/cooling power, and  $R_e$  is the effective radius of the particle ( $R_e = \sqrt[3]{3V/4\pi}$ , where  $V$  is the particle’s volume). In our experimental conditions  $V = 5 \times 10^{-18} \text{ m}^3$ ,  $R_e = 1.06 \times 10^{-6} \text{ m}$  and  $\kappa = 0.6 \text{ Wm}^{-1} \text{ K}^{-1}$ . From Figure 3c we get that the laser refrigeration obtained for a laser power of  $137 \times 10^{-3} \text{ W}$  is  $\Delta T = -6.8 \text{ K}$ . This, according to expression (5), gives a refrigeration power of

$$q = 4\pi\kappa R_e \Delta T = -5.4 \times 10^{-5} \text{ W} \quad (5)$$

This means that only a small ( $q/P_l = 4 \times 10^{-4}$ ) fraction of incident laser power is involved in the cooling process. This was, indeed, expected due to the low absorption coefficient characteristic of lanthanide ions (owing to the forbidden character of the optically active  $f-f$  transitions) and also due to the fact that 1020 nm radiation is far from the maximum absorption of ytterbium ions (see Figure S2, Supporting Information).<sup>[47]</sup> The absorption coefficient of ytterbium ions at 1020 nm in crystals is typically close to  $1 \text{ cm}^{-1}$  for a 5 at% doping level—this is approximately fourfold lower than found at 976 nm wavelength where the maximum is found.<sup>[48]</sup> According to the Lambert–Beer law and for a  $2.5 \text{ }\mu\text{m}$  thick particle, we estimate a single particle absorbance (the fraction of pump power that is absorbed by the microparticle) to be  $2.4 \times 10^{-4}$ . This is, indeed, very close to the fraction of incident pump power that is transformed into cooling power. This agreement supports the correctness of the use of angular deceleration to estimate the

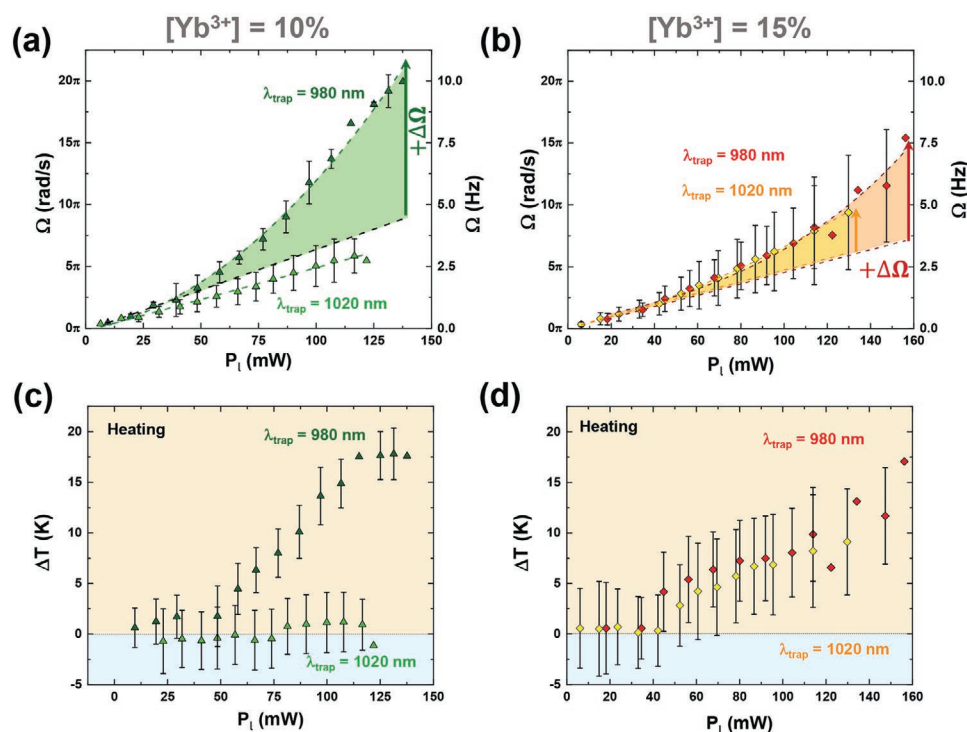


**Figure 4.** a,b) Power dependence of the spinning velocity of a 10 at% and a 15 at% doped  $\text{NaYF}_4:\text{Yb}^{3+}$  microparticle, respectively, as obtained for 980 and 1020 nm laser manipulation. The spinning velocity deviates from the low-power linear dependency, showing a supralinear behavior under 980 nm excitation for both samples and under 1020 nm excitation for the 15  $\text{NaYF}_4:\text{Yb}^{3+}$ . c) and d) show the power dependence of the temperature increment of a spinning particle under 980 and 1020 nm laser manipulation, respectively. Data were derived from (a) and (b) using the calibration curve of Figure S6 (Supporting Information).

magnitude of laser refrigeration. We note at this point that the laser refrigeration here found is  $\Delta T = -6.8$  K for an irradiance of  $7.5 \times 10^6 \text{ W cm}^{-2}$ . This leads to a maximum cooling efficiency of  $0.9 \times 10^{-6} \text{ KW}^{-1} \text{ cm}^2$ , which is very close to the magnitude of the laser refrigeration also reported for ytterbium-doped particles suspended in liquids for similar power densities (see Table S1, Supporting Information).

According to expression (5), the cooling magnitude is expected to increase with the fraction of laser power absorbed by the  $\text{NaYF}_4:\text{Yb}^{3+}$  particle, i.e., with the particle's absorption coefficient at 1020 nm. The easiest way to improve the absorption coefficient is increasing the amount of ytterbium ions. Thus, the possible presence of laser refrigeration was also investigated in 10 and 15 at% doped  $\text{NaYF}_4:\text{Yb}^{3+}$  microcrystals. In these cases the results obtained were different from those obtained for the 5 at% doped microcrystals. **Figure 4a** shows the laser power dependence of the spinning velocity of a 10 at% doped  $\text{NaYF}_4:\text{Yb}^{3+}$  microcrystal as obtained for both 980 and 1020 nm pumping. As with the 5 at% doped microcrystal, a clear supralinear trend is observed for 980 nm pumping indicating, as expected, relevant heating. At variance with the 5 at% microcrystal, the spinning velocity obtained when using the 1020 nm laser increases linearly with the laser power revealing the balance between the heating and cooling processes. The local temperature calculated from the experimental data included in **Figure 4a**, using the same procedure as in **Figure 3**, are depicted in **Figure 4b**. We found that 980 nm laser radiation causes a local heating of 17 K, whereas the local temperature remains

constant for 1020 nm pumping. Again, this is attributed to a balance between the cooling and heating processes. When the ytterbium content further increased, superlinear trends for both 980 and 1020 nm laser pumping were found (**Figure 4c**). This means that for such high ytterbium concentrations, net local heating is produced independently on the excitation wavelength. Indeed, the analysis of the data included in **Figure 4c** reveals that both 980 and 1020 nm pumping induces a very similar local heating (**Figure 4d**). In this case we state that for such high ytterbium concentration the heating induced by 1020 nm laser radiation overcomes the anti-Stokes emission induced cooling. **Figure 5a** summarizes the dependence of the induced change in local temperature achieved by both 980 and 1020 nm laser radiation on the ytterbium content. In all the cases, 980 nm laser radiation induces local heating whose magnitude does not follow a clear trend with the ytterbium concentration. This is, somehow, surprising. According to expression (5) local heating should be proportional to the amount of absorbed laser power and this, in turn, should increase with the ytterbium content. At this point this unexpected behavior can be attributed to two possible effects. First of all, the ytterbium content slightly affects the dimensions of the microparticles. As the ytterbium content increases (see Supporting Information), the microparticle thickness decreases well below the laser spot diameter ( $1.4 \mu\text{m}$ ). In such conditions a significant fraction of the laser beam is not overlapping with the microparticle volume so, for 10 and 15 at% doping levels, the actual incident laser power is smaller than the delivered laser power

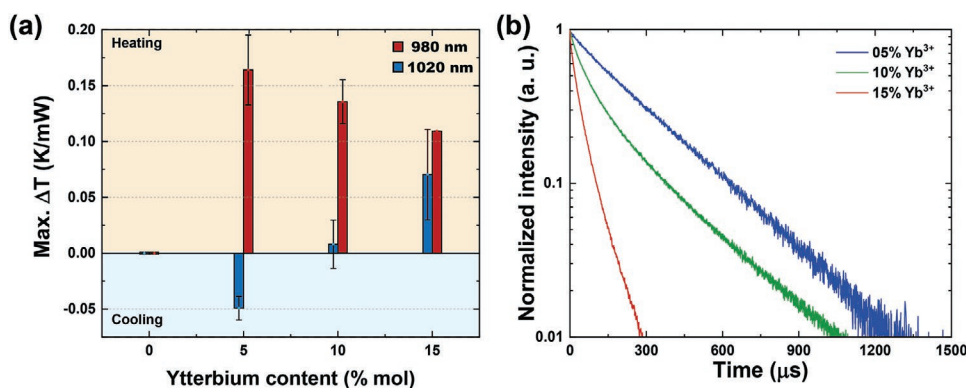


**Figure 5.** a) Maximum refrigeration and heating for each NaYF<sub>4</sub> microcrystal under 980 nm (red bars) and 1020 nm (blue bars) laser excitation. b) Fluorescence decay curves of the <sup>2</sup>F<sub>5/2</sub> Yb<sup>3+</sup> level in 5, 10 and 15 at% ytterbium-doped NaYF<sub>4</sub> microparticles.

that is actually used for comparison. The second explanation is related to the spectroscopic properties of various Yb<sup>3+</sup> content. Figure 5a reveals that the magnitude of 1020 nm laser refrigeration decreases significantly with the ytterbium content. Indeed, laser cooling is only observed for the 5 at% doping level. For the 10 at% doped sample, the microparticle remains at room temperature and for the 15 at% doped particle heating is observed instead of cooling. We state at this point that increasing ytterbium content above 5 at% induces the appearance of energy migration between ytterbium ions, facilitating effective energy transfer to quenching centers (most likely surface defect states or surface ligands). This hypothesis is supported by a relevant reduction of fluorescence lifetime in NaYF<sub>4</sub>: Yb<sup>3+</sup> microcrystals (Figure 5b). Since de-excitation at the quenching sites takes place by nonradiative transitions, the presence of this energy migration-induced quenching causes a net heating in the microcrystal that dominates over the anti-Stokes cooling.

It may also be relevant to consider the impact of pump laser wavelength, the external efficiency and the absorption efficiency on the cooling efficiency. Concerning the excitation wavelength—the more the pump wavelength is detuned from the E<sub>4</sub> → E<sub>5</sub> transition, the more vibronic energy will contribute or affect the system to balance the energy mismatches. However, because phonon emission is much more efficient than phonon absorption,<sup>[49]</sup> any detuning from this E<sub>4</sub> → E<sub>5</sub> transition (occurring at 1020 nm) will release optical phonons and this excess energy will contribute to heating, which in consequence will counterbalance the efficiency of optical cooling. The impact of the absorption efficiency and the external quantum efficiency of the phosphor on its cooling efficiency is also quite simple to predict in a qualitative manner. The higher the two values will be, the more pumping light will be absorbed and brighter emission will be achieved, which are beneficial for the optical cooling because the emitted photons simultaneously ‘carry’ excess of thermal energy (owing to phonon assistance) out of the luminescent crystal.

### 3. Conclusions

In summary, we demonstrate how it is possible to induce remote cooling at the microscale in fluids via anti-Stokes emission in an optically driven ytterbium-doped NaYF<sub>4</sub>

microparticle. Laser refrigeration is evidenced and evaluated by an analysis of the rotation dynamics of the NaYF<sub>4</sub> microparticle under circularly polarized laser beam, which experiences a relevant deceleration because cooling increases the medium viscosity. Under optimal conditions we have induced a local refrigeration by around 7 K for a pump laser of 1020 nm with a moderate power of 140 mW. These numbers are similar to those previously reported for other ytterbium-doped micro- and nanocrystals, although in our case we determined it by a simple and direct method—rotation dynamics of the cooling spinner.

It is also described how strongly the magnitude of laser refrigeration is dependent on the ytterbium content. We found that cooling is only efficient at moderate-low doping levels of 5 at%. We state that larger ytterbium concentrations induce energy migration and nonradiative de-excitations that behave as heating channels capable of balancing the anti-stokes cooling. A proper balance must be found between contrary effects the rising concentration of Yb(III) ions (Figures 3–5) may induce in the cooling spinners. On the one hand rising concentration enhance photon absorption at 1020 nm, where Yb absorption coefficient is significantly weaker than at its maximum at 980 nm. On the other hand, rising Yb(III) concentration, owing to relatively long radiative luminescence lifetime (≈1 ms) and large (≈10 000 cm<sup>−1</sup>) energy gap, is known to lead to efficient energy migration, which in consequence may transfer the excitation energy through the volume of the crystal to crystal defects or surface quenchers as well as may lead to multi-phonon relaxation with surface ligands and solvent. These latter phenomena are most probably observed for our microspinners (Figure S4, Supporting Information) where rising temperature leads to luminescence lifetime quenching down to <0.1 ms proportionally to the concentration of Yb(III). In the future, attempts to design a passive NaYF<sub>4</sub> shell around the Yb(III) doped NaYF<sub>4</sub> microspinners could potentially address the issues, observed in this work.

The results presented here open a new way of simultaneous controlling and monitoring temperature at the microscale in biocompatible fluids by a simple experimental approach. Therefore, these materials and methods can be of critical importance, for instance, in the control of cellular activity by simultaneous thermal and mechanical stimuli.

## 4. Experimental Section

**Materials and Synthesis of  $\beta$ -NaYF<sub>4</sub>: Yb<sup>3+</sup> Microparticles:** All of the chemical reagents in these experiments were used as received without further purification. Yttrium oxide (99.99%), ytterbium oxide (99.99%), and sodium fluoride were purchased from ALDRICH Chemistry. Ethanol (96% pure p.a.), sodium citrate (pure p.a.), and nitric acid (pure p.a.) were purchased from Avantor (Poland). Lanthanide nitrates were obtained by reactions stoichiometric amount of lanthanide oxides with nitric acid. Special care was taken to verify the purity of the reagents (especially ytterbium and yttrium oxides), as their potential contamination with other lanthanides (especially Er(III), which often accompany Yb(III) and Y(III) in raw lanthanide ores) could lead to parasitic energy transfer due to upconversion and could prevent successful demonstration of optical cooling. No such upconversion under 980 nm excitation was observed in the green spectra region, which confirmed high chemical purity of materials synthesized for the purpose of this work.

The NaYF<sub>4</sub> microparticles doped with Yb<sup>3+</sup> ions were prepared using the hydrothermal method. Typically, aqueous solutions of sodium citrate (9.31 mL; 0.3 M) and lanthanide nitrates (Ln(NO<sub>3</sub>)<sub>3</sub>, 14 mL; 0.2 M; Ln = Y, Yb) were mixed under vigorous stirring to form a milky suspension. Then, an aqueous solution of NaF (44.8 mL; 0.5 M) was added to form a transparent solution. The mixture was transferred to a 100 mL Teflon vessel and heated to 220 °C for 4 h. After cooling down to room temperature, the reaction product was isolated by centrifugation and washed with ethanol. Finally, the prepared particles were dispersed in water.

**Experimental System:** Single  $\beta$ -NaYF<sub>4</sub>: Yb<sup>3+</sup> microparticles were optically trapped using a homemade single beam optical trapping setup. 1020 and 980 nm linearly polarized single mode fiber-coupled laser diodes were used as laser radiation for both trapping and exciting the NaYF<sub>4</sub>: Yb<sup>3+</sup> microparticles. A quarter-wave plate was coupled before the focusing objective (NA = 0.85) to circularly polarize the laser beam and induce the microparticle's rotation. Its spinning velocity was obtained by recording the intensity fluctuations of the transmitted laser beam using a collector objective (NA = 0.25) coupled to a Position Sensitive Detector (PSD) and by analyzing them in the frequency domain (see Figure S6, Supporting Information). Additionally, a white LED and a CCD camera were incorporated to the single-beam optical trapping set-up, allowing real time visualization of the microparticle.

**Thermal Sensing:** The calibration curve was acquired by increasing the temperature of the deuterium oxide solution containing the optically trapped NaYF<sub>4</sub>: Yb<sup>3+</sup> microparticle with a heating plate, while recording the intensity fluctuations of transmitted laser beam with a PSD. More details can be found in the Supporting Information.

## Supporting Information

Supporting Information is available from the Wiley Online Library or from the author.

## Acknowledgements

This work was supported by the Ministerio de Ciencia e Innovación de España (PID2019-106211RB-I00 and PID2019-105195RA-I00) and by Universidad Autónoma de Madrid and Comunidad Autónoma de Madrid (S11/PJ1/2019-00052). E.O.R gratefully acknowledges the financial support provided by the Spanish Ministerio de Universidades, through the FPU program (FPU19/04803). K.P. acknowledges financial support from NCN, Poland, grant number 2018/31/D/ST5/01328.

## Conflict of Interest

The authors declare no conflict of interest.

## Data Availability Statement

The data that support the findings of this study are available from the corresponding author upon reasonable request.

## Keywords

laser refrigeration, NaYF<sub>4</sub>, optical cooling, optical trapping

Received: May 29, 2021

Revised: July 23, 2021

Published online: September 30, 2021

- [1] R. Yamanaka, Y. Shindo, K. Hotta, N. Hiroi, K. Oka, *Biochem. Biophys. Res. Commun.* **2020**, 533, 70.
- [2] B. U. S. Schmidt, T. R. Kießling, E. Warmt, A. W. Fritsch, R. Stange, J. A. Käs, *New J. Phys.* **2015**, 17, 073010.
- [3] H. Mao, T. Yang, P. S. Cremer, *J. Am. Chem. Soc.* **2002**, 124, 4432.
- [4] J. Sadeghi, A. H. B. Ghasemi, H. Latifi, *Lab Chip* **2016**, 16, 3957.
- [5] H. Li, X. Wang, T. Y. Ohulchanskyy, G. Chen, **2021**, 33, 2000678.
- [6] X. Zhou, B. E. Smith, P. B. Roder, P. J. Pauzauskie, *Adv. Mater.* **2016**, 28, 8658.
- [7] P. P. Fedorov, V. B. Aleksandrov, O. S. Bondareva, I. I. Buchinskaya, M. D. Val'kovskii, B. P. Sobolev, *Crystallogr. Rep.* **2001**, 46, 239.
- [8] A. Grzechnik, P. Bouvier, W. A. Crichton, L. Farina, J. Köhler, *Solid State Sci.* **2002**, 4, 895.
- [9] R. Kumar, M. Nyk, T. Y. Ohulchanskyy, C. A. Flask, P. N. Prasad, *Adv. Funct. Mater.* **2009**, 19, 853.
- [10] G. Liang, H. Wang, H. Shi, H. Wang, M. Zhu, A. Jing, J. Li, G. Li, *J. Nanobiotechnol.* **2020**, 18, 154.
- [11] P. Rodríguez-Sevilla, Y. Zhang, P. Haro-González, F. Sanz-Rodríguez, F. Jaque, J. G. Solé, X. Liu, D. Jaque, *Adv. Mater.* **2016**, 28, 2421.
- [12] E. Ortiz-Rivero, K. Prorok, M. Skowicki, D. Lu, A. Bednarkiewicz, D. Jaque, P. Haro-González, *Small* **2019**, 15, 1904154.
- [13] M. Runowski, N. Stopikowska, D. Szeremeta, S. Goderski, M. Skwierczyńska, S. Lis, *ACS Appl. Mater. Interfaces* **2019**, 11, 13389.
- [14] S. Xu, S. Xu, Y. Zhu, W. Xu, P. Zhou, C. Zhou, B. Dong, H. Song, *Nanoscale* **2014**, 6, 12573.
- [15] Q. Guo, J. Wu, Y. Yang, X. Liu, J. Jia, J. Dong, Z. Lan, J. Lin, M. Huang, Y. Wei, Y. Huang, *J. Power Sources* **2019**, 426, 178.
- [16] F. Xu, Y. Sun, H. Gao, S. Jin, Z. Zhang, H. Zhang, G. Pan, M. Kang, X. Ma, Y. Mao, *ACS Appl. Mater. Interfaces* **2021**, 13, 2674.
- [17] D. Kumar, S. K. Sharma, S. Verma, V. Sharma, V. Kumar, *Mater. Today* **2020**, 21, 1868.
- [18] Y. Tang, W. Di, X. Zhai, R. Yang, W. Qin, *ACS Catal.* **2013**, 3, 405.
- [19] P. Mazierski, J. K. Roy, A. Mikolajczyk, E. Wyrzykowska, T. Grzyb, P. N. A. Caicedo, Z. Wei, E. Kowalska, A. Zaleska-Medynska, J. Nadolna, *Appl. Surf. Sci.* **2021**, 536, 147805.
- [20] M. Haase, H. Schäfer, *Angew. Chem., Int. Ed.* **2011**, 50, 5808.
- [21] A. D. Pickel, A. Teitelboim, E. M. Chan, N. J. Borys, P. J. Schuck, C. Dames, *Nat. Commun.* **2018**, 9, 4907.
- [22] Y. Li, B. Chen, L. Tong, X. Zhang, S. Xu, X. Li, J. Zhang, J. Sun, X. Wang, Y. Zhang, G. Sui, Y. Zhang, X. Zhang, H. Xia, *Results Phys.* **2019**, 15, 102704.
- [23] G. Chen, H. Qiu, P. N. Prasad, X. Chen, *Chem. Rev.* **2014**, 114, 5161.
- [24] S. Bigotta, D. Parisi, L. Bonelli, A. Toncelli, A. D. Lieto, M. Tonelli, *Opt. Mater.* **2006**, 28, 1321.
- [25] G. Nemova, R. Kashyap, *J. Lumin.* **2015**, 164, 99.



- [26] D. V. Seletskiy, S. D. Melgaard, R. I. Epstein, A. Di Lieto, M. Tonelli, M. Sheik-Bahae, *Opt. Express* **2011**, 19, 18229.
- [27] J. Thiede, J. Distel, S. R. Greenfield, R. I. Epstein, *Appl. Phys. Lett.* **2005**, 86, 154107.
- [28] J. Fernández, A. Mendioroz, A. J. García, R. Balda, J. L. Adam, *J. Alloys Compd.* **2001**, 323–324, 239.
- [29] B. Zhong, Y. Lei, H. Luo, Y. Shi, T. Yang, J. Yin, *J. Lumin.* **2020**, 226, 117472.
- [30] X. Xia, A. Pant, A. S. Ganas, F. Jelezko, P. J. Pauzauskie, *Adv. Mater.* **2021**, 33, 1905406.
- [31] R. I. Epstein, M. I. Buchwald, B. C. Edwards, T. R. Gosnell, C. E. Mungan, *Nature* **1995**, 377, 500.
- [32] A. T. M. A. Rahman, P. F. Barker, *Nat. Photonics* **2017**, 11, 634.
- [33] P. B. Roder, B. E. Smith, X. Zhou, M. J. Crane, P. J. Pauzauskie, *Proc. Natl. Acad. Sci. USA* **2015**, 112, 15024.
- [34] X. Xia, A. Pant, X. Zhou, E. A. Dobretsova, A. B. Bard, M. B. Lim, J. Y. D. Roh, D. R. Gamelin, P. J. Pauzauskie, *Chem. Mater.* **2021**, 33, 4417.
- [35] X. Liang, X. Wang, J. Zhuang, Q. Peng, Y. Li, *Adv. Funct. Mater.* **2007**, 17, 2757.
- [36] C. Li, Z. Quan, J. Yang, P. Yang, J. Lin, *Inorg. Chem.* **2007**, 46, 6329.
- [37] X. Shan, F. Wang, D. Wang, S. Wen, C. Chen, X. Di, P. Nie, J. Liao, Y. Liu, L. Ding, P. J. Reece, D. Jin, *Nat. Nanotechnol.* **2021**, 16, 531.
- [38] V. I. Sokolov, A. V. Zvyagin, S. M. Igumnov, S. I. Molchanova, M. M. Nazarov, A. V. Nechaev, A. G. Savelyev, A. A. Tyutyunov, E. V. Khaydukov, V. Y. Panchenko, *Opt. Spectrosc.* **2015**, 118, 609.
- [39] P. Rodríguez-Sevilla, Y. Zhang, P. Haro-Gonzalez, F. Sanz-Rodríguez, F. Jaque, J. G. Sole, X. Liu, D. Jaque, *Adv. Mater.* **2016**, 28, 2421.
- [40] P. Rodríguez-Sevilla, H. Rodríguez-Rodríguez, M. Pedroni, A. Speghini, M. Bettinelli, J. G. Solé, D. Jaque, P. Haro-González, *Nano Lett.* **2015**, 15, 5068.
- [41] P. Rodríguez-Sevilla, T. Lee, L. Liang, P. Haro-González, G. Lifante, X. Liu, D. Jaque, *Adv. Opt. Mater.* **2018**, 6, 1800161.
- [42] E. Ortiz-Rivero, M. Skowicki, K. Prorok, D. Lu, T. Lipinski, A. Bednarkiewicz, D. Jaque, P. Haro-González, **2020**, 16, 2002055.
- [43] M. Hosseinzadeh, F. Hajizadeh, M. Habibi, H. M. Moghaddam, S. N. S. Reihani, *Appl. Phys. Lett.* **2018**, 113, 223701.
- [44] P. Rodríguez-Sevilla, Y. Arita, X. Liu, D. Jaque, K. Dholakia, *ACS Photonics* **2018**, 5, 3772.
- [45] P. Haro-González, W. T. Ramsay, L. M. Maestro, B. del Rosal, K. Santacruz-Gomez, M. del Carmen Iglesias-de la Cruz, F. Sanz-Rodríguez, J. Y. Chooi, P. R. Sevilla, M. Bettinelli, D. Choudhury, A. K. Kar, J. G. Solé, D. Jaque, L. Paterson, *Small* **2013**, 9, 2162.
- [46] G. Baffou, R. Quidant, F. J. García de Abajo, *ACS Nano* **2010**, 4, 709.
- [47] M. P. Hehlen, M. G. Brik, K. W. Krämer, *J. Lumin.* **2013**, 136, 221.
- [48] A. K. Rufino Souza, A. P. Langaro, J. R. Silva, F. B. Costa, K. Yukimitu, J. C. Silos Moraes, L. Antonio de Oliveira Nunes, L. Humberto da Cunha Andrade, S. M. Lima, *J. Alloys Compd.* **2019**, 781, 1119.
- [49] N. Yamada, S. Shionoya, T. Kushida, *J. Phys. Soc. Jpn.* **1972**, 32, 1577.